Stochastic Modeling of Carbon Oxidation

Wei-Yin Chen, Advait Kulkarni, and Jeremy L. Milum
Dept. of Chemical Engineering, University of Mississippi, University, MS 38677

L. T. Fan
Dept. of Chemical Engineering, Kansas State University, Manhattan, KS 66506

Recent studies of carbon oxidation by scanning tunneling microscopy indicate that measured rates of carbon oxidation can be affected by randomly distributed defects in the carbon structure, which vary in size. Nevertheless, the impact of this observation on the analysis or modeling of the oxidation rate has not been critically assessed. This work focuses on the stochastic analysis of the dynamics of carbon clusters' conversions during the oxidation of a carbon sheet. According to the classic model of Nagle and Strickland-Constable (NSC), two classes of carbon clusters are involved in three types of reactions: gasification of basal-carbon clusters, gasification of edge-carbon clusters, and conversion of the edge-carbon clusters to the basal-carbon clusters due to thermal annealing. To accommodate the dilution of basal clusters, however, the NSC model is modified for the later stage of oxidation in this work. Master equations governing the numbers of three classes of carbon clusters, basal, edge and gasified, are formulated from stochastic population balance. The stochastic pathways of the three different classes of carbon during oxidation, that is, their means and the fluctuations around these means, have been numerically simulated independently by the algorithm derived from the master equations, as well as by an event-driven Monte Carlo algorithm. Both algorithms have given rise to identical results.

Introduction

The dual-site, Langmuir-Hinshelwood model of carbon oxidation, developed by Blyholder et al. (1958) and its modified version by Nagle and Strickland-Constable (1962), or the NSC model in short, have been widely adopted for modeling carbon oxidation. The features and applicability of the NSC model have been extensively discussed in several reviews (such as Laurendeau, 1978; Essenhigh, 1981; Suuberg, 1991). Nevertheless, it is deemed desirable to reassess the validity of the NSC model in the light of additional information on carbon oxidation and new data obtained with various types of carbon and experimental apparatus.

The experimental setups of Blyholder et al. (1958) and Nagle and Strickland-Constable (1962) included impinging oxygen or a nitrogen/oxygen mixture onto the face containing the basal planes of a carbon-black rod heated by electric current. The carbon was consumed layer by layer, and the rate of oxidation was determined by measuring microscopically the position of the carbon surface. In analyzing the data and deriving models based on them, the rate of carbon oxidation is assumed to be controlled partly by the adsorption of oxygen molecules and atoms, and partly by the desorption of two classes of carbon−oxygen complexes derived from carbon of two different structural characteristics in the graphite. These structurally different classes of carbon have been termed the edge carbon and the basal carbon in the combustion literature.

Chu and Schmidt (1992, 1993) induced physically fresh defects in the basal plan of the carbon structure and examined the formation and growth of pits after oxidation by scanning tunneling microscopy. At relatively low temperatures, they observed that the pits originated at defective sites, or edges. The abstraction of basal carbon by oxygen was possible at higher temperatures (> 700°C). To calibrate the instrument's sensitivity, the surface was randomly imaged first in an area 15×15 μm^2 in size for about 20 different regions of each crystal; each imaged area contained approximately 675 to 900

Correspondence concerning this article should be addressed to Wei-Yin Chen.

pits. They have observed a wide range of pit sizes after oxidation of basal carbon. The oxidation rate per unit area was determined by averaging the data over several crystals with 150 to 200 pits recorded in a typical measurement. To estimate the total area of all the single-layer pits, they have considered a 10-nm segment as the fundamental unit in discretizing the pit-size distribution, which corresponds to approximately the length of 30 diameters of carbon atoms. These studies clearly indicate that the sizes of pits in the samples are mesoscopic in nature. Inevitably, this renders the fluctuations appreciable in the estimated or predicted rates based on the measurements; thus, a stochastic analysis is indeed warranted.

Recently, Kyotani et al. (1996) conducted Monte Carlo simulations of the oxidation of a carbon sheet where the gasification probability of each carbon atom was determined by the Huckel molecular orbital theory. In other words, the conversions and their fluctuations were simulated in their study; they depend mainly on the carbon structure at the atomic level. For the oxidation of a defected carbon sheet, however, the inherent fluctuations can also arise from the random, mesoscopic defects in the carbon structure; these fluctuations have manifested themselves in the observation of pits formation and in the measurement of the oxidation rate conducted by Chu and Schmidt (1992, 1993). Analysis of these fluctuations requires that we resort to a very different approach, that is, the stochastic analysis, mentioned at the conclusion of the preceding paragraph.

The primary objective of the present work is to conduct stochastic analysis and modeling of the carbon oxidation process where the rate is governed by the mesoscopic defects in the carbon structure; the classic dual-site view of the carbon structure of the NSC model is adopted. Mathematically, the stochastic algorithm follows what has been established by Oppenheim et al. (1977), Gardiner (1985), and van Kampen (1992, pp. 96–133).

Model Formulation

The system under consideration includes a sheet of graphite carbon and its oxidation products in the gas phase. The carbon sheet comprises both the crystalline-carbon, that is, basal-carbon, clusters, and the clusters of carbon around dispersed defects, that is, edge-carbon clusters. These clusters have equal collision frequencies with the oxygen in the gas phase. According to the NSC model, these two classes of carbon clusters undergo three types of reactions: the gasification of edge-carbon clusters, the gasification of basal-carbon clusters, and the conversion of edge-carbon clusters to basal-carbon clusters via thermal annealing. For brevity, the basal-carbon clusters, the edge-carbon clusters, and their gasified products will be simply referred to as the basal, edge, and gasified clusters, respectively, hereafter. To analyze the mesoscopic size of the pits, a fundamental measuring unit needs to be identified. The fundamental unit, or size, of a cluster is dictated by factors such as the sizes of the defects, the segment length adopted in discretizing the pit-size distribution in reporting and analyzing the experimental data, and by the instrument's sensitivity; as noted in the preceding section, Chu and Schmidt (1992) have considered a 10-nm segment as the fundamental unit. Once the cluster size is identified, the quantity of carbon in a cluster is defined for all three types of carbon clusters.

The carbon sheet discussed here contains a limited carbon source, and, thus, the three types of carbon clusters just defined form a closed system. In what follows, we shall discuss the carbon-rod system of Nagle and Strickland-Constable (1962), which is of the open-flow type, and the steady-state hypothesis of the NSC model. In our extension of the NSC model to the carbon sheet, the steady-state hypothesis must be removed.

During the entire experiment for oxidizing carbon on the surface of a graphite rod, only a small amount of carbon is usually gasified from an essentially unlimited source of carbon in the graphite. In the analysis based on the NSC model, the material balance is performed over a carbon surface exposed to the oxygen jet under the assumption that the system is at a steady state, that is, the ratio of the two classes of carbon remains constant on the exposed surface. The system is of the open-flow type since the gasification of a unit of either basal or edge cluster instantaneously brings a neighboring, unexposed basal cluster into the system, that is, the exposed surface, as an edge cluster. The conversions of carbon clusters to the exposed surface are the sole sources of edge clusters; therefore, the gasification of an edge cluster does not change the distribution of cluster numbers in the system. The thermal annealing and gasification of basal clusters are the sole source and sink of basal clusters, respectively; thus, operating the open-flow system under a steady state requires that the rate of gasification of basal clusters be equal to that of their thermal annealing.

The rate of carbon gasification is considered to be the sum of the gasification rates of edge carbon and basal carbon, which are coupled through the common factor, x, representing the fraction of edge carbon on the surface. The steady-state assumption just discussed suggests that the factor, x, can be determined by equating the rate of gasification of basal carbon and that of thermal annealing. It is interesting to note that the direct experimental verification of the factor, x, in the NSC model has not been reported in the literature; nevertheless, the dual-site view of carbon surface forms the basis in the development of the concepts and experimental methodologies for measuring the active surface and reactive surface areas during carbon oxidation (Lizzio et al., 1990).

Blyholder et al. (1958) have chosen 1 and 2 for the numbers of basal sites to be converted to an edge site when an edge cluster and a basal cluster are gasified from the exposed surface, respectively. The number of secondary conversion of basal sites to edge sites during the gasification of a basal site, 2, apparently has been assigned by taking into account not only the conversion of the basal cluster underneath the newly gasified cluster, but also the conversion of a neighboring cluster on the same plane. Blyholder et al. have stated that the selection is arbitrary and the results of calculation are insensitive to the selection in their system. This value has been reduced to 1 in the NSC model. For the carbon sheet discussed in the present work, however, the supply of carbon for secondary reactions comes only from the carbons in the same plane. Thus, for modeling the oxidation of a carbon sheet we assume that the gasification of a cluster of basal or edge carbon instantaneously results in the conversion of a neighboring, unexposed basal cluster to an edge cluster.

The oxidation rates of soot particles have been measured with a shock-tube reactor (such as Park and Appleton, 1973) and flow reactors (Neoh et al., 1981; Felder et al., 1988). These rates have been compared with those of the NSC model. The steady-state hypothesis of the NSC model is valid because the extent of the carbon conversion in the reactors mentioned earlier is sufficiently low. Naturally, the steady-state hypothesis is valid only up to a certain level of carbon conversion. Toward the end of the oxidation process, particularly for the porous particles, basal carbon sites are mostly isolated in the carbon matrix and the gasification of a cluster of basal or edge carbon is not expected to instantaneously result in the conversion of a neighboring, unexposed basal cluster to an edge cluster. Hence, the NSC model is also expected to overpredict the conversion. To extend the prediction to the entire carbon burnout process, a model is developed in the current work for the later stage of combustion where the basal clusters are assumed to be completely isolated.

Let the random variables, $N_1(t)$, $N_2(t)$, and $N_3(t)$, represent the numbers of the basal, edge, and gasified clusters. Consequently, the random vector of the system is $N(t) = [N_1(t), N_2(t), N_3(t)]^T$, where T stands for the transpose. The realization of the random vector, $n(t) = [n_1(t), n_2(t), n_3(t)]^T$, represents the state of the system at time t. The probability that the system be in state n at time t is denoted by $P_{n_1, n_2, n_3}(t)$ or $P[n_1(t), n_2(t), n_3(t); t]$. The following assumptions are imposed in deriving the master equations governing the transition of the system among various states.

1. The random vector, $N(t)$, is Markovian, that is, for any set of successive times $t_1 < t_2 < \cdots < t_q$, we have $P[N(t_q)|N(t_1), N(t_2), \ldots, N(t_{q-1})] = P[N(t_q)|N(t_{q-1})]$ (such as Parzen, 1962).

2. The number of cluster conversion depends only on the time interval, that is, it is temporally homogeneous, signifying that $N(\Delta t)$ and $[N(t + \Delta t) - N(t)]$ are identically distributed.

3. The probability of an arbitrary cluster to undergo one type of reaction is proportional to the time interval $(t, t + \Delta t)$, if the interval Δt is sufficiently small.

4. The probability of a cluster to make more than one transition is zero during the time interval $(t, t + \Delta t)$ so that at most one transition occurs during this period.

The transition-intensity functions, λ_i's are defined on the basis of the preceding assumptions as follows:

$$\Pr\left[\text{a basal cluster will gasify during the time interval, } (t, t+\Delta t)\right] = \lambda_1 \Delta t + o(\Delta t) \quad (1)$$

$$\Pr\left[\text{an edge cluster will gasify during the time interval, } (t, t+\Delta t)\right] = \lambda_2 \Delta t + o(\Delta t) \quad (2)$$

$$\Pr\left[\text{an edge cluster will convert to a basal cluster during the time interval, } (t, t+\Delta t)\right] = \lambda_3 \Delta t + o(\Delta t), \quad (3)$$

where

$$\lim_{\Delta t \to 0} \frac{o(\Delta t)}{\Delta t} = 0. \quad (4)$$

The definitions of the transition-intensity functions, Eqs. 1 through 3, render it possible to perform a probabilistic population balance around a particular state of the system by taking into account the mutually exclusive events probably occurring during the evolution of the system. Since the dynamics of the two stages differ from each other, they are discussed separately below. It is also worth mentioning that these transition-intensity functions are the major parameters defining the rate of carbon oxidation dynamics; they form the basis not only of deriving the master equations, but also of constructing the Monte Carlo procedure, as will be elaborated later.

First stage

For four mutually exclusive events leading the evolution of the state of the system include the following.

1. A basal cluster gasifies, thus giving rise to a gasified cluster and an edge cluster (see Figure 1).
2. An edge cluster gasifies, thereby yielding a gasified cluster and another edge cluster (see Figure 2).
3. An edge cluster is converted to a basal cluster through thermal annealing (see Figure 3).
4. None of these events takes place.

As illustrated in Figure 4, the probabilities that the four mutually exclusive events occurring at arbitrary time t will lead the system to state n at time $(t + \Delta t)$ can be written as

$$\Pr\left[\text{the system will transform into state } n \text{ from another state due to the gasification of a basal cluster during the time interval, } (t, t+\Delta t)\right] = (n_1 + 2)\lambda_1 \Delta t P_{n_1+2, n_2-1, n_3-1}(t) + o(\Delta t) \quad (5)$$

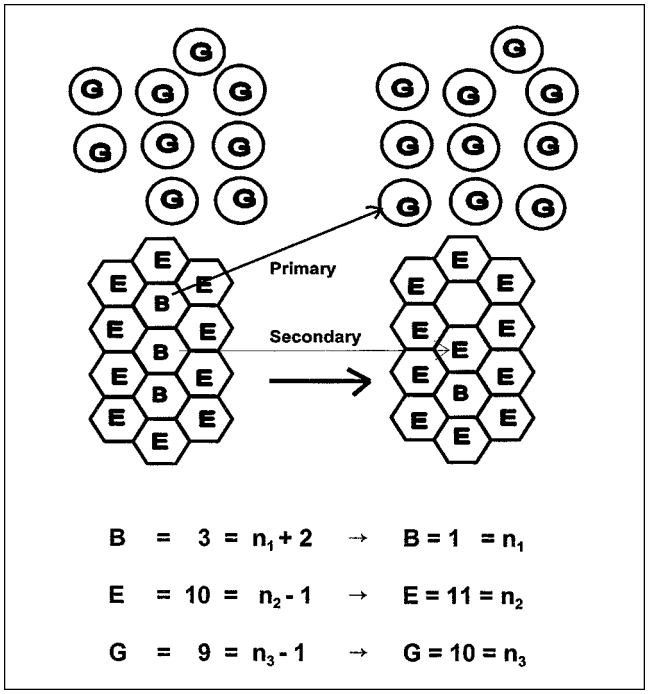

Figure 1. Gasification of a basal-carbon cluster in the first stage of the modified NSC model.

B = basal-carbon cluster; E = edge-carbon cluster; G = gasified-carbon cluster.

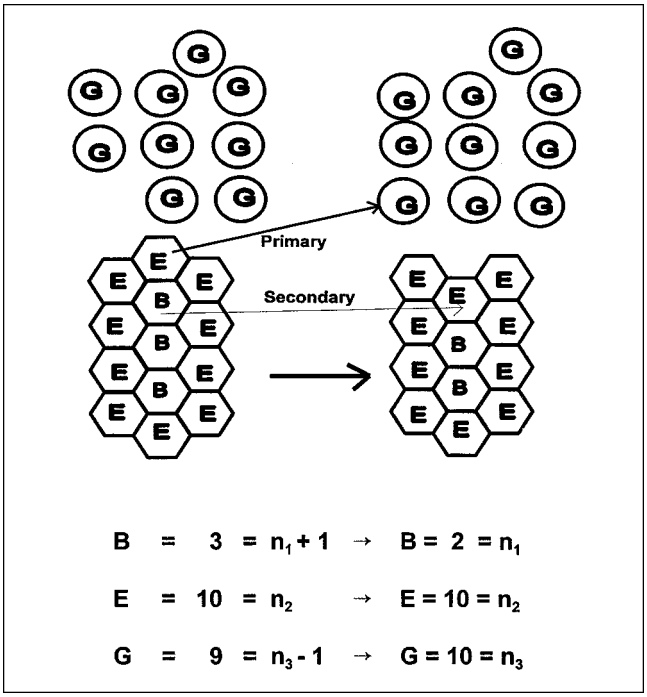

Figure 2. Gasification of an edge-carbon cluster in the first stage of the modified NSC model.

B = basal-carbon cluster; E = edge-carbon cluster; G = gasified-carbon cluster.

$$\Pr\left[\text{the system will transform into state } n \text{ from another state due to the gasification of an edge cluster during the time interval, } (t, t+\Delta t)\right] = n_2\lambda_2\Delta t P_{n_1+1,\,n_2,\,n_3-1}(t) + o(\Delta t) \tag{6}$$

$$\Pr\left[\text{the system will transform into state } n \text{ from another state due to the thermal annealing of an edge cluster to a basal cluster during the time interval, } (t, t+\Delta t)\right] = (n_2+1)\lambda_3\Delta t P_{n_1-1,\,n_2+1,\,n_3}(t) + o(\Delta t) \tag{7}$$

$$\Pr\left[\text{the system will remain at state } n \text{ during the time interval, } (t, t+\Delta t)\right] = \left[1-(n_1\lambda_1 + n_2\lambda_2 + n_2\lambda_3)\Delta t\right]P_{n_1,\,n_2,\,n_3}(t) + o(\Delta t). \tag{8}$$

By summing all the probabilities, Eqs. 5 through 8, we obtain the probability that the system is at state n at arbitrary time $(t+\Delta t)$ as follows:

$$P_{n_1,\,n_2,\,n_3}(t+\Delta t) = (n_1+2)\lambda_1\Delta t P_{n_1+2,\,n_2-1,\,n_3-1}(t) + n_2\lambda_2\Delta t P_{n_1+1,\,n_2,\,n_3-1}(t) + (n_2+1)\lambda_3\Delta t P_{n_1-1,\,n_2+1,\,n_3}(t) + \left[1-(n_1\lambda_1 + n_2\lambda_2 + n_2\lambda_3)\Delta t\right]P_{n_1,\,n_2,\,n_3}(t) + o(\Delta t) \tag{9}$$

Rearranging the preceding equation and taking the limit as

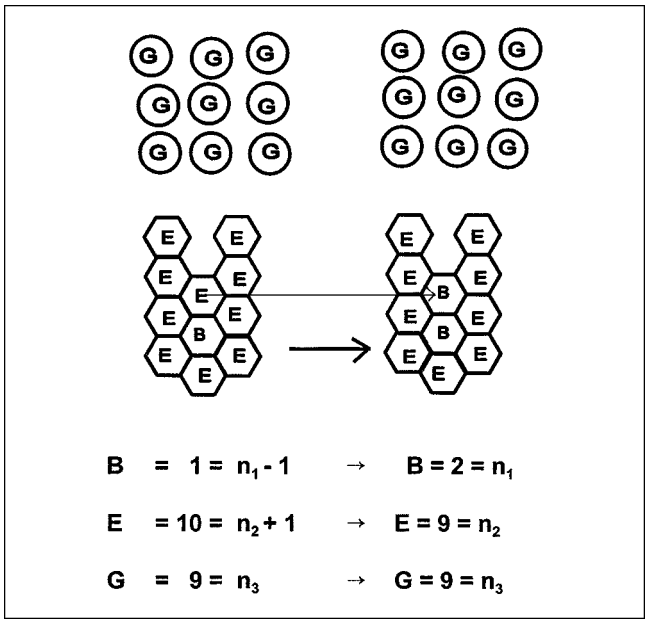

Figure 3. Thermal annealing of an edge-carbon in the first stage of the modified NSC model.

B = basal-carbon cluster; E = edge-carbon cluster; G = gasified-carbon cluster.

$\Delta t \to 0$ result in the following master equation governing the first stage of the oxidation:

$$\frac{dP_n(t)}{dt} = (n_1+2)\lambda_1 P_{n_1+2,\,n_2-1,\,n_3-1}(t) + n_2\lambda_2 P_{n_1+1,\,n_2,\,n_3-1}(t) + (n_2+1)\lambda_3 P_{n_1-1,\,n_2+1,\,n_3}(t) - (n_1\lambda_1 + n_2\lambda_2 + n_2\lambda_3)P_{n_1,\,n_2,\,n_3}(t). \tag{10}$$

For convenience, the one-step operator, D, is introduced here; it is defined through its effect on arbitrary function $f(n)$ as (van Kampen, 1992, p. 139)

$$Df(n) = f(n+1) \qquad \text{and} \qquad D^{-1}f(n) = f(n-1). \tag{11}$$

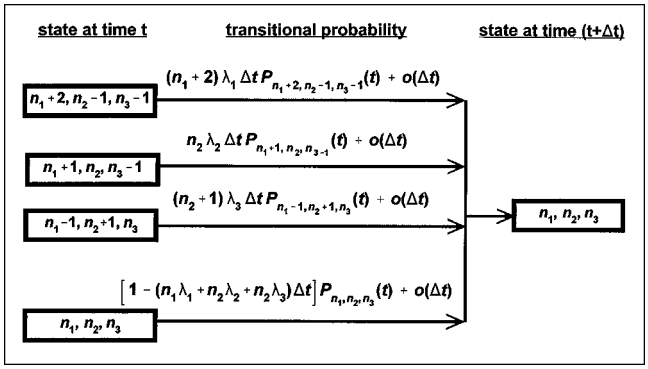

Figure 4. Probability balance involving four mutually exclusive events in the time interval $(t, t+dt)$ in the first stage.

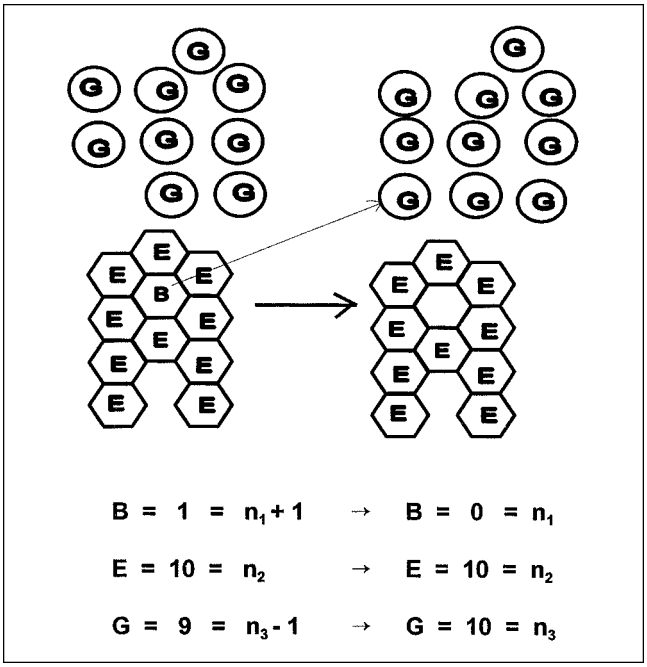

Figure 5. Gasification of a basal-carbon cluster in the second stage of the modified NSC model.

B = basal-carbon cluster; E = edge-carbon cluster; G = gasified-carbon cluster.

In light of this definition, the master equation, Eq. 10, is rewritten in compact form as shown below:

$$\frac{dP_n(t)}{dt} = \lambda_1\left(D_{n_1}^2 D_{n_2}^{-1} D_{n_3}^{-1} - 1\right) n_1 P_n(t) + \lambda_2\left(D_{n_1} D_{n_3}^{-1} - 1\right) n_2 P_n(t) + \lambda_3\left(D_{n_1}^{-1} D_{n_2} - 1\right) n_2 P_n(t). \quad (12)$$

Second stage

The four mutually exclusive events causing the evolution of the state of the system include the following.

1. A basal cluster gasifies, thus giving rise to a gasified cluster (see Figure 5).
2. An edge cluster gasifies, thereby yielding a gasified cluster (see Figure 6).
3. An edge cluster is transformed into a basal cluster through thermal annealing (see Figure 7).
4. None of these events takes place.

As summarized in Figure 8, the probabilities that these four mutually exclusive events occurring at the second stage of the process will lead the system to state n at an arbitrary time t can be written as

$$\Pr\left[\text{the system will transform into state } n \text{ from another state due to the gasification of a basal cluster during the time interval, } (t, t+\Delta t)\right] = (n_1+1)\lambda_1 \Delta t P_{n_1+1,\, n_2,\, n_3-1}(t) + o(\Delta t) \quad (13)$$

$$\Pr\left[\text{the system will transform into state } n \text{ from another state due to the gasification of an edge cluster during the time interval, } (t, t+\Delta t)\right] = (n_2+1)\lambda_2 \Delta t P_{n_1,\, n_2+1,\, n_3-1}(t) + o(\Delta t) \quad (14)$$

$$\Pr\left[\text{the system will transform into state } n \text{ from another state due to the thermal annealing of an edge cluster during the time interval, } (t, t+\Delta t)\right] = (n_2+1)\lambda_3 \Delta t P_{n_1-1,\, n_2+1,\, n_3}(t) + o(\Delta t) \quad (15)$$

$$\Pr\left[\text{the system will remain at state } n \text{ during the time interval, } (t, t+\Delta t)\right] = \left[1-(n_1\lambda_1 + n_2\lambda_2 + n_2\lambda_3)\Delta t\right] P_{n_1,\, n_2,\, n_3}(t) + o(\Delta t) \quad (16)$$

By summing all the probabilities given (Eqs. 13 through 16) we obtain the probability that the system is at state n at arbitrary time $(t+\Delta t)$ as follows:

$$P_{n_1,\, n_2,\, n_3}(t+\Delta t) = (n_1+1)\lambda_1 \Delta t P_{n_1+1,\, n_2,\, n_3-1}(t) + (n_2+1)\lambda_2 \Delta t P_{n_1,\, n_2+1,\, n_3-1}(t) + (n_2+1)\lambda_3 \Delta t P_{n_1-1,\, n_2+1,\, n_3}(t) + \left[1-(n_1\lambda_1 + n_2\lambda_2 + n_2\lambda_3)\Delta t\right] P_{n_1,\, n_2,\, n_3}(t) + o(\Delta t). \quad (17)$$

Rearranging the preceding equation and taking the limit as

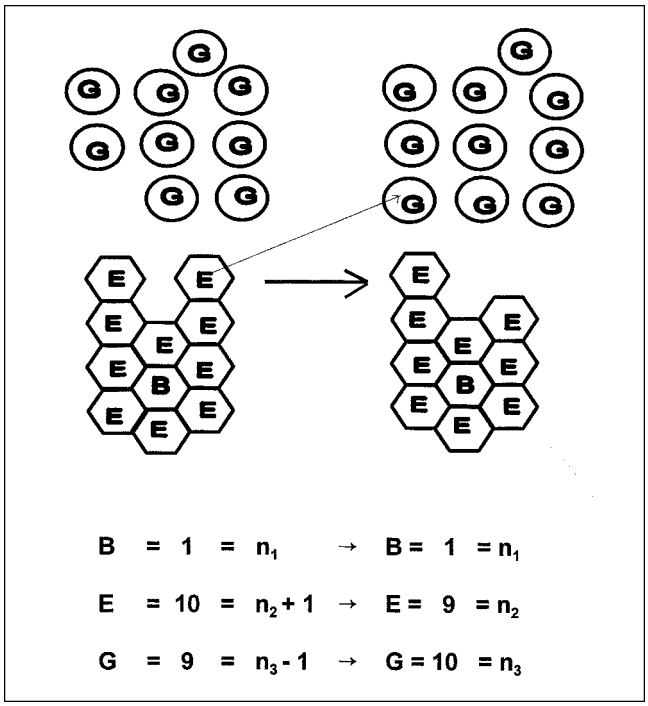

Figure 6. Gasification of an edge-carbon cluster in the second-stage of the modified NSC model.

B = basal-carbon cluster; E = edge-carbon cluster; G = gasified-carbon cluster.

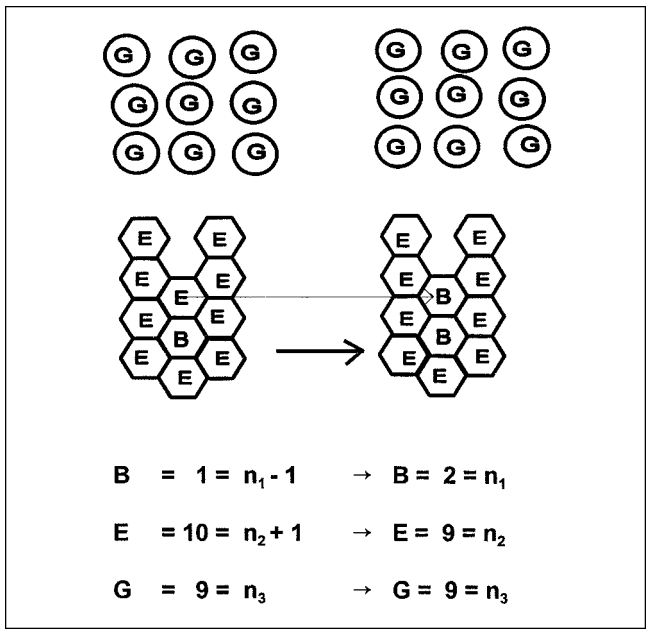

Figure 7. Thermal annealing of an edge-carbon in the second stage of the modified NSC model.

B = basal-carbon cluster; E = edge-carbon cluster; G = gasified-carbon cluster.

$\Delta t \to 0$ result in the following master equation governing the second stage of the oxidation.

$$\frac{dP_n(t)}{dt} = (n_1+1)\lambda_1 P_{n_1+1,\,n_2,\,n_3-1}(t) + (n_2+1)\lambda_2 P_{n_1,\,n_2+1,\,n_3-1}(t) + (n_2+1)\lambda_3 P_{n_1-1,\,n_2+1,\,n_3}(t) - (n_1\lambda_1 + n_2\lambda_2 + n_2\lambda_3) P_{n_1,\,n_2,\,n_3}(t). \quad (18)$$

On the basis of the definition of D (Eq. 11) this equation is rewritten compactly as

$$\frac{dP_n(t)}{dt} = \lambda_1\left(D_{n_1}D_{n_3}^{-1}-1\right)n_1 P_n(t) + \lambda_2\left(D_{n_2}D_{n_3}^{-1}-1\right)n_2 P_n(t) + \lambda_3\left(D_{n_1}^{-1}D_{n_2}-1\right)n_2 P_n(t). \quad (19)$$

The master equations (Eqs. 12 and 19) comprise two sets of coupled linear ordinary differential equations with the joint probability function, $P_n(t)$, as its unknown. Each equation in the set represents a particular outcome n. Even though the linear master equations, Eq. 12 or 19, can be analytically solved by the method of the joint-probability-generating function (such as Chiang, 1980), it is extremely difficult, if not impossible, to do so because of the exceedingly large number of possible n's. In practice, however, it often suffices to determine only the expressions for the first and second moments of the resultant cluster-size distribution. These moments, in turn, yield the expressions for the means, variances, and covariances that can be correlated or compared with the experimental data. The equations governing the moments are derived through an averaging technique, which is discussed in the next section.

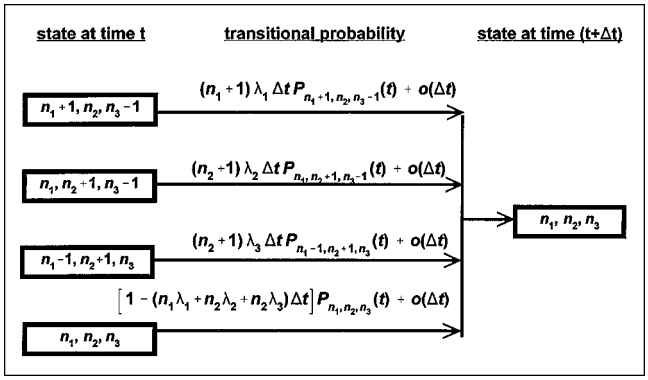

Figure 8. Probability balance involving four mutually exclusive events in the time interval $(t, t+dt)$ in the second stage.

Means, variances, and covariances

The equations governing the means, variances, and covariances of the N_i have been derived by generating the first and second moments of the master equations for the both stages of oxidation. They are separately presented.

First Stage. Multiplying both sides of the master equation (Eq. 12) by n_i, and rearranging the resultant expression lead to the following equations governing the first moments or means of the random variables:

$$\frac{dE[N_1(t)]}{dt} = -2\lambda_1 E[N_1(t)] - \lambda_2 E[N_2(t)] + \lambda_3 E[N_2(t)] \quad (20)$$

$$\frac{dE[N_2(t)]}{dt} = \lambda_1 E[N_1(t)] - \lambda_3 E[N_2(t)] \quad (21)$$

$$\frac{dE[N_3(t)]}{dt} = \lambda_1 E[N_1(t)] + \lambda_2 E[N_2(t)]. \quad (22)$$

Multiplying both sides of the master equation (Eq. 12) by n_i^2, and rearranging the resultant expression yields the following equations governing the second moments of the random variables of the first stage:

$$\frac{dE[N_1^2(t)]}{dt} = -4\lambda_1\left(E[N_1^2(t)] - E[N_1(t)]\right) - \lambda_2\left(2E[N_1(t)N_2(t)] - E[N_2(t)]\right) + \lambda_3\left(2E[N_1(t)N_2(t)] + E[N_2(t)]\right) \quad (23)$$

$$\frac{dE[N_2^2(t)]}{dt} = \lambda_1\left(2E[N_1(t)N_2(t)] + E[N_1(t)]\right) - \lambda_3\left(2E[N_2^2(t)] - E[N_2(t)]\right) \quad (24)$$

$$\frac{dE[N_3^2(t)]}{dt} = \lambda_1\left(2E[N_1(t)N_3(t)] + E[N_1(t)]\right) + \lambda_2\left(2E[N_2(t)N_3(t)] + E[N_2(t)]\right). \quad (25)$$

By multiplying both sides of the master equation (Eq. 12), by $(n_i n_j)$, and rearranging the resultant expression, we obtain the equations governing the cross moments of two random variables of the first stage as follows:

$$\frac{dE[N_1(t)N_2(t)]}{dt} = \lambda_1\big(-2E[N_1(t)N_2(t)] - 2E[N_1(t)] + E[N_1^2(t)]\big) - \lambda_2\big(E[N_2^2(t)]\big) - \lambda_3(E[N_1(t)N_2(t)] - E[N_2^2(t)] + E[N_2(t)]) \quad (26)$$

$$\frac{dE[N_2(t)N_3(t)]}{dt} = \lambda_1(E[N_1(t)N_2(t)] + E[N_1(t)] + E[N_1(t)N_3(t)]) + \lambda_2\big(E[N_2^2(t)]\big) - \lambda_3(E[N_2(t)N_3(t)]) \quad (27)$$

$$\frac{dE[N_1(t)N_3(t)]}{dt} = \lambda_1\big(-2E[N_1(t)N_3(t)] - 2E[N_1(t)] + E[N_1^2(t)]\big) + \lambda_2(-E[N_2(t)N_3(t)] + E[N_1(t)N_2(t)] - E[N_2(t)]) + \lambda_3(E[N_2(t)N_3(t)]). \quad (28)$$

Solving Eqs. 20 through 28 simultaneously gives the first and second moments of $N_i(t)$. The variances around the means, $\mathrm{Var}[N_i(t)]$, and the covariances around the means, $\mathrm{Cov}[N_i, N_j]$, can be obtained from the following formulas (Casella and Berger, 1990, pp. 58, 161):

$$\mathrm{Var}[N_i(t)] = E\big[(N_i(t) - E[N_i(t)])^2\big]$$

or

$$\mathrm{Var}[N_i(t)] = E[N_i^2(t)] - (E[N_i(t)])^2 \quad (29)$$

and

$$\mathrm{Cov}[N_i(t), N_j(t)] = E\big[(N_i(t) - E[N_i(t)])(N_j(t) - E[N_j(t)])\big]$$

or

$$\mathrm{Cov}[N_i(t), N_j(t)] = E[N_i(t)N_j(t)] - E[N_i(t)]E[N_j(t)]. \quad (30)$$

The first terms on the righthand sides of Eqs. 23 and 24 can be obtained from the equations for the second moments of N_i and N_j; and the second terms, from the equations for the first moments or means of N_i.

Second Stage. The equations governing the moments for the second stage can be derived through an approach similar to that for the first stage. Multiplying both sides of the master equation (Eq. 19) by n_i, and rearranging the resultant expression, leads to the following equations governing the first moments or means of the random variables of the second stage.

$$\frac{dE[N_1(t)]}{dt} = -\lambda_1 E[N_1(t)] + \lambda_3 E[N_2(t)] \quad (31)$$

$$\frac{dE[N_2(t)]}{dt} = -\lambda_2 E[N_2(t)] - \lambda_3 E[N_2(t)] \quad (32)$$

$$\frac{dE[N_3(t)]}{dt} = \lambda_1 E[N_1(t)] + \lambda_2 E[N_2(t)]. \quad (33)$$

Multiplying both sides of Eq. 19 by n_i^2, and rearranging the resultant expression leads to the following equation governing the second moments of the random variables of the second stage:

$$\frac{dE[N_1^2(t)]}{dt} = \lambda_1\big(-2E[N_1^2(t)] + E[N_1(t)]\big) + \lambda_3(2E[N_1(t)N_2(t)] + E[N_2(t)]) \quad (34)$$

$$\frac{dE[N_2^2(t)]}{dt} = \lambda_2\big(-2E[N_2^2(t)] + E[N_2(t)]\big) + \lambda_3\big(-2E[N_2^2(t)] + E[N_2(t)]\big) \quad (35)$$

$$\frac{dE[N_3^2(t)]}{dt} = \lambda_1(E[N_1(t)] + 2E[N_1(t)N_3(t)]) + \lambda_2(2E[N_2(t)N_3(t)] + E[N_2(t)]). \quad (36)$$

By multiplying both sides of Eq. 19 by $(n_i n_j)$ and rearranging the resultant expression, we have the equations governing the cross moments of two random variables of the second stage as follows:

$$\frac{dE[N_1(t)N_2(t)]}{dt} = -\lambda_1(E[N_1(t)N_2(t)]) - \lambda_2(E[N_1(t)N_2(t)]) - \lambda_3(E[N_1(t)N_2(t)] - E[N_2^2(t)] + E[N_2(t)]) \quad (37)$$

$$\frac{dE[N_2(t)N_3(t)]}{dt} = +\lambda_1(E[N_1(t)N_2(t)]) + \lambda_2(E[N_2^2(t)] - E[N_2(t)N_3(t)] - E[N_2(t)]) - \lambda_3(E[N_2(t)N_3(t)]) \quad (38)$$

$$\frac{dE[N_1(t)N_3(t)]}{dt} = \lambda_1(-E[N_1(t)N_3(t)] + E[N_1^2(t)] - E[N_1(t)]) + \lambda_2(E[N_1(t)N_2(t)]) + \lambda_3(E[N_2(t)N_3(t)]). \quad (39)$$

Similar to the random variables of the first stage, solving Eqs. 31 through 39 simultaneously gives the first and second moments of $N_i(t)$. The variances around the means, $\mathrm{Var}[N_i(t)]$,

and the covariances around the means, Cov$[N_i, N_j]$, can be estimated by means of Eqs. 29 and 30.

Simulation

The two-stage model presented in the preceding section has been simulated by two approaches. The first relies on the solution of the governing equations for the first and second moments of the random variables derived from the master equations, or the master-equation algorithm in brief, and the second resorts to the event-driven Monte Carlo algorithm. The values of the parameters characterizing the dynamics of oxidation are estimated prior to the simulation.

Assessment of system parameters

The oxidation process of interest is characterized by the transition-intensity function, λ_i, defining the probability of cluster conversion per unit time due to reaction i (see Eqs. 1 through 3). If the fraction of cluster converted per unit time is taken to represent this intensity function, its significance is equivalent to the deterministic rate constant, k. In other words, from the change in the total number of clusters attributable to reaction i during the time interval $(t, t+\Delta t)$ we have

$$-R_i = \lim_{\Delta t \to 0} \frac{n - \left[n - n\lambda_i \Delta t + o(\Delta t)\right]}{\Omega \Delta t} = \lambda_i (n/\Omega), \quad (40)$$

where Ω stands for the system size, for example, surface area for a surface oxidation system; and $-R_i$, the number of clusters converted attributable to reaction type i per unit time per unit area. A detailed discussion of the relationship between the rate constant and the intensity function can be found in van Kampen (1992, p. 166). Equation 40 implies that the rate of cluster conversion obeys the first-order law.

The transition-intensity functions have been estimated from the rate expressions of Nagle and Strickland-Constable (1962). For the gasification of edge clusters, the rate is considered to be limited by the adsorption of oxygen and desorption of surface oxygen complexes, thus leading to the following rate expression in s^{-1}.

$$R_A = \frac{k_A p}{1 + K_z p} x, \quad (41)$$

where

k_A = product of oxidation-rate constant for edge clusters in the Arrhenius form and K_z
$= 20 \exp[-30{,}000(\text{cal/mol})/(\text{RT})]$, in $\text{g} \cdot \text{cm}^{-2} \cdot \text{s}^{-1} \cdot \text{atm}^{-1}$
K_z = adsorption–desorption equilibrium constant
$= 21.3 \exp[4{,}100(\text{cal/mol})/(\text{RT})]$, in atm^{-1}
x = fraction of edge clusters on the carbon surface
p = partial pressure of oxygen, in atm.

Various mechanistic studies, however, have revealed that the gasification of edge carbon should not be considered to follow a simple Langmuir-Hinshelwood mechanism (such as von Fredersdorff and Elliott, 1963; Spokes and Benson, 1967; Laurendeau, 1978; Suuberg, 1991); the detailed mechanism is more complex, and Eq. 41 can only be regarded as an approximation.

For the gasification of basal clusters, Nagle and Strickland-Constable have regarded the rate to be governed by the interaction between oxygen and basal clusters, thereby leading to the following rate expression in s^{-1}:

$$R_B = k_B p(1 - x), \quad (42)$$

where

k_B = oxidation-rate constant for basal clusters in Arrhenius form
$= 4.46 \times 10^{-3} \exp[-15{,}200(\text{cal/mol})/(\text{RT})]$, in $\text{g} \cdot \text{cm}^{-2} \cdot \text{s}^{-1} \cdot \text{atm}^{-1}$.

For the conversion of edge clusters due to thermal annealing, Nagle and Strickland-Constable have determined that the rate depends on the fraction of edge clusters on the carbon surface. This leads to the following rate expression in s^{-1}:

$$R_T = k_T x, \quad (43)$$

where

k_T = rate constant for thermal annealing in Arrhenius form
$= 1.51 \times 10^{-5} \exp(-97{,}000(\text{cal/mol})/(\text{RT}))$, in $\text{g} \cdot \text{cm}^{-2} \cdot \text{s}^{-1}$.

By assuming that each basal carbon occupies the same area as an edge carbon atom, 8.3 Å^2 (Laine et al., 1963), the rate expressions (Eqs. 41 through 43), can be converted from the surface-area basis to the atomic or cluster basis. Under arbitrarily selected conditions defined by a temperature of 1,800 K and an oxygen partial pressure of 0.23 atm, the λ_i's have been evaluated as

$$\lambda_1 = \frac{k_A p}{1 + K_z p} = 626.4 \text{ s}^{-1} \quad (44)$$

$$\lambda_2 = k_B p = 2{,}809 \text{ s}^{-1} \quad (45)$$

$$\lambda_3 = k_T = 12.49 \text{ s}^{-1}. \quad (46)$$

The simulations have been carried out with these values of λ_i. The temperature and oxygen partial pressure are chosen well within the range of the conditions of Nagle and Strickland-Constable (1962), where the experimental data and model predictions are shown to be in good accord. Under these conditions, the steady-state assumption of Nagle and Strickland-Constable implies that the fraction of edge carbon on the carbon surface is high during combustion of graphite rod:

$$x = \frac{1}{1 + \dfrac{k_T}{k_B p}} = 0.9945.$$

This is consistent with their interpretation that thermal annealing becomes an important reaction and the basal function on the graphite surface becomes notable only above 2,100 K.

Simulation based on the master equations

To simulate the temporal profiles of the three clusters in the first stage, Eqs. 20 through 30 have been solved simultaneously. Among these equations, Eqs. 20 through 22 are for the means; Eqs. 23 through 25, for the second moments; and

Eqs. 26 through 28, for the cross moments. The variances and covariances have been recovered from Eqs. 29 and 30, respectively. The linear system of differential equations, Eqs. 20 through 28, can be solved either by an analytical method, such as the method of eigenvalue/eigenvector problems, or by a numerical method. For the present work, it has been simultaneously solved on a SGI Origin 200 computer with LSODA, a software package based on Gear's method for solving a set of ordinary differential equations (Petzold and Hindmarsh, 1997).

To investigate the effect of the number of initial carbon clusters, five sets of computations were conducted with five initial clusters of 40, 100, 240, 400 and 800 in number. The ratio of the basal to edge clusters is kept constant at 19 to 1 throughout these computations. Equations 20 through 28 have been integrated to a point at which the basal clusters become highly diluted. To estimate the ''breaking point'' between the two stages, a deterministic model involving a continuous decrease in the frequency of the occurrence of the secondary reaction is developed for comparison. It is envisioned that the occurrence of the secondary reaction depends on the identity of the cluster adjacent to the gasifying cluster, and the frequency of occurrence depends on the parameter ϵ, the fraction of basal clusters in the carbon sheet after a cluster is gasified, or $n_1/(n_1+n_2)$. Material balance yields three equations governing the three types of carbon clusters during combustion; only the equation governing the number of basal clusters is shown below:

$$\frac{dn_1}{dt} = -\lambda_1(1+\epsilon)n_1 - \lambda_2\epsilon n_2 + \lambda_3 n_2.$$

Comparing the cluster numbers from this approach and those from the two-stage approach with varying breakpoints, the breaking point yielding the most compatible cluster numbers in the second stage is chosen through visual comparison. For the current work, gasification is switched to the second stage when $\epsilon = 0.3$; the corresponding time is 0.727 ms.

To simulate the temporal profiles of three clusters in the second stage, the linear system of differential equations (Eqs. 31 through 39) has been simultaneously integrated by LSODA with the system's state at the end of the first stage serving as the initial condition for the second stage. Among these equations, Eqs. 31 through 33 are for the means; Eqs. 34 through 36, for the second moments; and Eqs. 37 through 39, for the cross moments. The variances and covariances have been recovered from Eqs. 29 and 30, respectively.

Monte Carlo simulation

Linear or nonlinear dynamic processes have been simulated either deterministically or stochastically by Monte Carlo procedures. It is worth noting that a well-developed class of Monte Carlo simulation procedures essentially shares identical computational bases with the master-equation algorithm presented in the preceding sections. Specifically, the assumptions of Markov property and temporal homogeneity of the random variables lead to the definitions of transition-intensity functions (such as Gillespie, 1977, 1992). As discussed in the Model Formulation section, probability balances of various events on the basis of these intensity functions give rise to the master equations. In the Monte Carlo simulation, the system's state is simulated by a stepwise, random-walk scheme based on the same intensity functions.

Process systems or phenomena can be simulated by time-driven and event-driven Monte Carlo procedures (such as Rajamani et al., 1986). The difference between these two procedures is in the manner of updating the time clock of the evolution of the system. The time-driven procedure advances the simulation clock by a prespecified time increment, Δt, which is sufficiently small so that at most one event will occur in this interval. The probability of an event occurring is determined by the nature of the transition-intensity functions. In contrast, the event-driven procedure updates the simulation clock by randomly generating the waiting time, τ_w, which has an exponential distribution; this distribution signifies that a cluster transition takes place completely randomly. At the end of the each waiting interval, one event will occur, and the state to which the system will transfer is also determined by the nature of the transition-intensity functions.

The process of interest here, that is, carbon oxidation, has been simulated by the event-driven procedure; it is usually computationally faster than the time-driven procedure. The simulation starts with a given initial distribution of clusters; the essential task is to obtain the probability distributions of the cluster numbers at any subsequent times. To determine the system transition in each time step, two random numbers are generated for two different purposes. The first random number in $(0,1)$, r_1, is for estimating the waiting time during which a possible transitions of the system's state, depicted in Figure 4 or 8, will take place. The second random number in $(0,1)$, r_2, is for identifying the reaction type.

Waiting Time. Let T_n be the random variable representing the waiting time of the carbon system of interest at state n prior to its transition due to the transformation of an arbitrary carbon cluster, and let τ_w be the realization of T_n. Moreover, let $G_n(\tau_w)$ be the probability that no transition occurs during the time interval, τ_w. Thus,

$$G_n(\tau_w) = \Pr(T_n \geq \tau_w), \tag{47}$$

which can be expressed as

$$G_n(\tau_w) = \exp\left[-(n_1\lambda_1 + n_2\lambda_2 + n_2\lambda_3)\tau_w\right]. \tag{48}$$

The complement of $G_n(\tau_w)$,

$$H_n(\tau_w) = 1 - G_n(\tau_w), \tag{49}$$

expresses the cumulative probability distribution of T_n up to τ_w. The probability-density function of T_n,

$$h(\tau_w) \equiv \frac{dH_n(\tau_w)}{d\tau_w},$$

therefore, has the following exponential form.

$$h(\tau_w) = (n_1\lambda_1 + n_2\lambda_2 + n_2\lambda_3) \times \exp\left[-(n_1\lambda_1 + n_2\lambda_2 + n_2\lambda_3)\tau_w\right]. \tag{50}$$

Note that, $H_n(\tau_w)$ is the probability function of T_n.

Equation 50 indicates that to estimate the waiting time of the carbon cluster, τ_w, a sequence of exponentially distributed random numbers must be generated. The sequences of the computer-generated random numbers, however, are usually uniformly distributed in interval [0, 1]. This uniform distribution, therefore, needs to be transformed into the exponential distribution, which can be accomplished by defining a new random variable, denoted by U, whose realization, denoted by u, assumes the value of $H_n(\tau_w)$ at τ_w (such as Gillespie, 1992), that is,

$$u = H_n(\tau_w) = 1 - \exp\left[-(n_1\lambda_1 + n_2\lambda_2 + n_2\lambda_3)\tau_w\right], \quad (51)$$

or, inversely,

$$\tau_w = \frac{-1}{(n_1\lambda_1 + n_2\lambda_2 + n_2\lambda_3)} \ln[1-u]. \quad (52)$$

It can be verified that if the waiting time, T_n, whose realization is τ_w, is exponentially distributed, then the random variable, U, whose realization is u, is uniformly distributed over interval [0, 1].

Probabilities of Three Possible Transitions. After residing in state $n = (n_1, n_2, n_3)$ for a waiting time of τ_w, the carbon system will transfer to one of its adjacent states. During the first stage of the oxidation, the transition intensities of the carbon system from state (n_1, n_2, n_3) to state $(n_1-2,\ n_2+1,\ n_3+1)$, $(n_1-1,\ n_2,\ n_3+1)$, and $(n_1+1,\ n_2-1,\ n_3)$ are λ_1, λ_2, and λ_3, respectively; this is the total reverse but the exact equivalent of the system transition from states $(n_1+2,\ n_2-1,\ n_3-1)$, $(n_1+1,\ n_2,\ n_3-1)$, and $(n_1-1,\ n_2+1,\ n_3)$ to state (n_1, n_2, n_3) is illustrated in Figure 4. During the second stage of the oxidation, the transition intensities of the carbon system from state (n_1, n_2, n_3) to (n_1-1, n_2, n_3+1), (n_1, n_2-1, n_3+1), and (n_1+1, n_2-1, n_3) are λ_1, λ_2, and λ_3, respectively; as depicted in Figure 8. The probability of the carbon system transferring from state (n_1, n_2, n_3) to (n_1-2, n_2+1, n_3+1) during the first stage or to (n_1-1, n_2, n_3+1) during the second stage, therefore, is

$$Q_1 = \frac{n_1\lambda_1}{n_1\lambda_1 + n_2\lambda_2 + n_2\lambda_3}. \quad (53)$$

The probability of the carbon system transferring from state (n_1, n_2, n_3) to (n_1-1, n_2, n_3+1) during the first stage or to (n_1, n_2-1, n_3+1) during the second stage is

$$Q_2 = \frac{n_2\lambda_2}{n_1\lambda_1 + n_2\lambda_2 + n_2\lambda_3}. \quad (54)$$

Similarly, the probability of the carbon system transferring from state (n_1, n_2, n_3) to (n_1, n_2-1, n_3+1) during either the first or second stage is

$$Q_3 = \frac{n_2\lambda_3}{n_1\lambda_1 + n_2\lambda_2 + n_2\lambda_3}. \quad (55)$$

It is worth mentioning that even though the states to which the system is converting differ for two stages, the three criteria for determining the reaction step are identical: they are Eqs. 53 through 55. Since the sum of Q_1 through Q_3 is 1, the reaction type can be identified by the randomly generated number, r_2. Specifically, r_2 falling within the interval

$$\left[0, \frac{n_1\lambda_1}{(n_1\lambda_1 + n_2\lambda_2 + n_2\lambda_3)}\right] \quad (56)$$

implies that a basal cluster is gasified; r_2 falling within the interval

$$\left[\frac{n_1\lambda_1}{(n_1\lambda_1 + n_2\lambda_2 + n_2\lambda_3)}, \frac{n_1\lambda_1 + n_2\lambda_2}{(n_1\lambda_1 + n_2\lambda_2 + n_2\lambda_3)}\right] \quad (57)$$

implies that an edge cluster is gasified; and r_2 falling within the interval

$$\left[\frac{n_1\lambda_1 + n_2\lambda_2}{(n_1\lambda_1 + n_2\lambda_2 + n_2\lambda_3)}, 1\right] \quad (58)$$

implies that thermal annealing occurs.

Simulation Algorithm. A stepwise description of the event-driven procedure is given below.

1. Choose an initial cluster distribution, and let the number of replications, S, be the sum of initial basal and edge clusters. Start the random walk from this state.

2. Select the total length of time of each simulation, T_f. For convenience, T_f has been selected as 3.7 ms.

3. Determine the length of waiting time, τ_w. First, generate a random number, r_1, from a uniform distribution in [0, 1]; then, calculate τ_w for a system's transition at state (n_1, n_2, n_3) according to Eq. 52.

4. Update the computer clock by letting $t = t + \tau_w$.

5. Calculate the transition probabilities that the system will transfer from state n to the other states, Q_i, by Eqs. 53 through 55. Then, generate another random number, r_2, from a uniform distribution in [0, 1]. Determine the reaction type by examining in which interval given by Eqs. 56 through 58 is r_2 located.

6. Repeat steps 3 through 5 until the total time exceeds T_f; this terminates one replication of simulation.

7. Repeat steps 2 through 6 for S times, and store the resultant number of clusters of type i during the jth replication at time t, $n_{ij}(t)$. This yields the mean number of clusters of type i at time t:

$$E[N_i(t)] = \frac{\sum_{j=1}^{S} n_{ij}}{S}. \quad (59)$$

The variance of clusters of type i at time t can be calculated from its definition:

$$\mathrm{Var}[N_i(t)] = \frac{\sum_{j=1}^{S} \left(n_{ij} - E[N_i(t)]\right)^2}{S-1}. \quad (60)$$

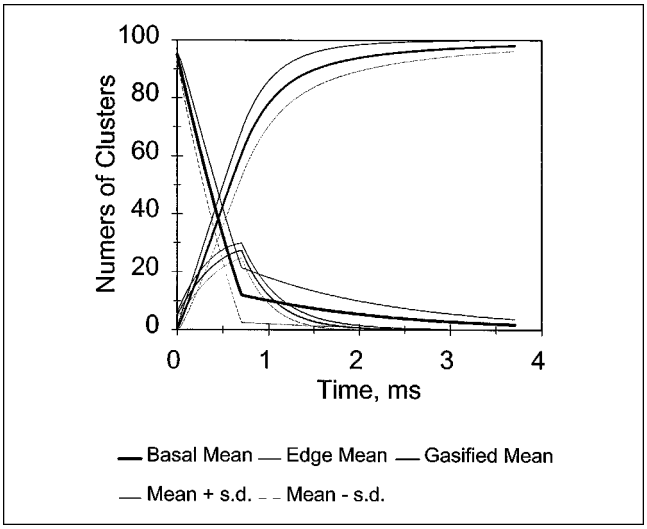

Figure 9. Temporal evolutions of the three types of carbon clusters and their standard-deviation envelops.

From the simulation of a carbon sheet containing 100 clusters computed independently by the master-equation and Monte Carlo algorithms.

The covariance around the means between any two types of clusters, i and j, at time t can be calculated from its definition:

$$\mathrm{Cov}\left[N_i(t), N_j(t)\right] = \frac{\sum_{h=1}^{S}\sum_{k=1}^{S}\left(n_{ih} - E\left[N_i(t)\right]\right)\left(n_{jk} - E\left[N_j(t)\right]\right)}{S-1}. \quad (61)$$

Results and Discussion

The current work proposes a novel, two-stage model of carbon oxidation by extending the classical NSC model. A stochastic analysis of the proposed model has yielded the transition probabilities or, more specifically, transition-intensity functions, of gasification and transformation of carbon clusters during oxidation. This renders it possible to derive the master equations of the model through stochastic population balance and to derive the event-driven Monte Carlo procedure for the model, both of which enable the model to be simulated independent of each other.

Simulation based on the master equations

Figure 9 presents the temporal profiles of oxidation of basal and edge clusters from the simulations with 100 total initial clusters and an initial ratio of basal-to-edge clusters of 19:1. It is worth noting that the number of basal clusters decreases continuously until the second stage is reached at 0.727 ms. If the calculation is not switched to the second stage at this moment, the rate of the consumption of basal clusters remains negative, and the number of basal clusters will eventually become negative. In fact, the eigenvalues of the matrix of the differential equations governing the means in the first stage, Eqs. 20 through 22, include a set of complex conjugates indicating oscillations in the numbers of clusters. This implies that the assumptions of the secondary, instantaneous conversion of basal to edge clusters during the first stage of the oxidation is too restrictive after the basal clusters are highly diluted, and thus, the assumptions must be removed in the second stage.

The envelopes of standard deviation around the means in Figure 9 are indicative of the internal, or system, fluctuations (van Kampen, 1992, p. 234). The master equations resulting from the stochastic analysis of a complex process facilitate the estimation of these fluctuations. The parameters in the equations, for example, the intensity functions, are presumed to depend only on the major variables of the system and to be independent of the variables of secondary importance. Neglecting these secondary variables is, in essence, the source of internal noises that should be appropriately analyzed stochastically. For the current work, the transition-intensity functions, corresponding to the reaction rates, are functions of temperature and oxygen pressure, but are independent of the local characteristics of the defects. The fluctuations around the means increase rapidly with time and then decline slowly; they finally vanish as expected because of the total consumption of carbon.

The covariances around the means between the two types of clusters are plotted in Figure 10; note that the interactions between the numbers of the two types of clusters can be appreciable. The covariances, similar to the variances, are quantities that cannot be evaluated *a priori* by a deterministic model.

Figure 11 presents the temporal profiles of oxidation of basal and edge clusters from the simulations with the total initial clusters of 400 and an initial ratio of basal-to-edge clusters of 19:1. The mean evolutions of cluster numbers are proportional to those demonstrated in Figure 9, because the

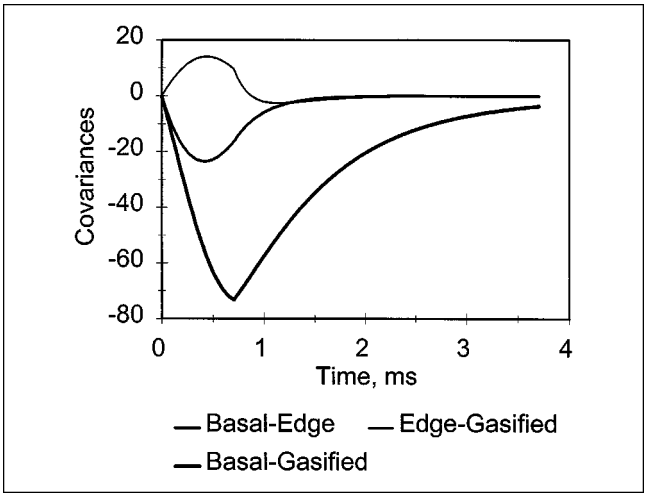

Figure 10. Temporal evolutions of the three covariances.

From the simulation of a carbon sheet containing 100 clusters computed independently by the master-equation and Monte Carlo algorithms.

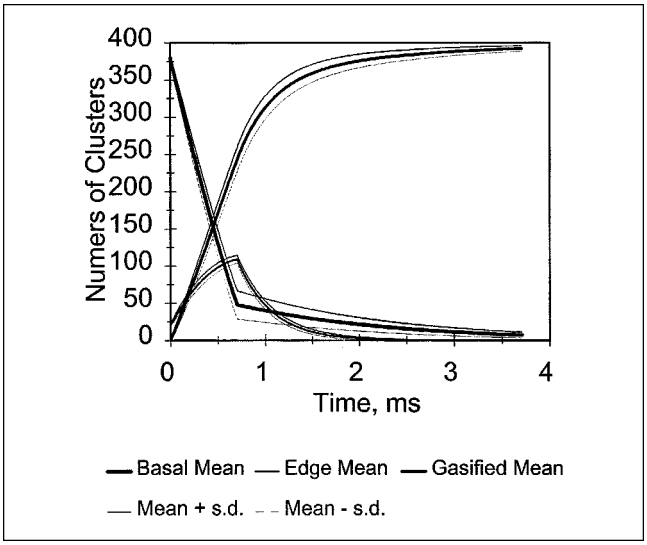

Figure 11. Temporal evolutions of the three types of carbon clusters and their standard-deviation envelops.

From the simulation of a carbon sheet containing 400 clusters computed independently by the master-equation and Monte Carlo algorithms.

macroscopic equations, Eqs. 20 through 22 and Eqs. 31 through 33, are linear. Nevertheless, the deviations from the means are significantly smaller than those in Figure 9, thereby indicating that the fluctuations decrease with the increase in the initial number of clusters. Indeed, this trend is particularly noticeable when the maximum variances from each of the five simulations are plotted against the initial cluster number (see Figure 12). This observation is also in accordance with the theory of stochastic analysis that the internal noises are particularly noticeable when the number of entities is small (such as Nicolis and Prigogine, 1977; van Kampen, 1992, pp. 55–58 and 232–235).

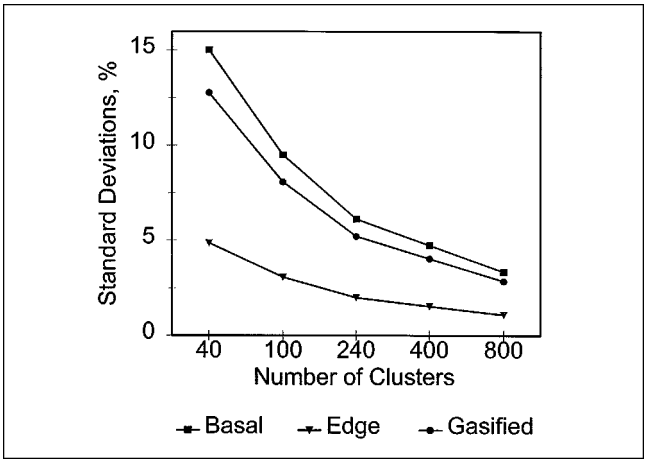

Figure 12. Variations of the standard deviations with the initial number of clusters.

Computed independently by the master-equation and Monte Carlo algorithms.

Simulation based on the Monte Carlo procedure

Monte Carlo simulations have yielded results essentially indistinguishable from those generated from the master equations, that is, those shown in Figures 9 through 12. As discussed earlier, this is expected since the algorithms based on the event-driven Monte Carlo procedure and master equations derived in the present work are rooted in identical assumptions, that is, the Markov property and temporal homogeneity of the random variables. These assumptions lead to the definitions of transition-intensity functions that are the cornerstones of the formulation of the master equations and of the Monte Carlo procedure. Three traces from the Monte Carlo simulations, one for each carbon cluster, are included in Figure 9 for comparison.

Although the master-equation algorithm and the Monte Carlo algorithm share common assumptions, they are independent of each other. The fact that the two algorithms have yielded essentially the same results implies that both indeed define the evolution of a dynamic process in a precisely equivalent way. The master-equation algorithm generates the equations governing the statistical moments of the process, which can be readily varied to cover a wide range of initial conditions, whereas the Monte Carlo procedure will require far more computational time and storage space under such circumstances.

The current model demonstrates that the macroscopic route and internal fluctuations of the carbon oxidation process can be predicted by resorting to a limited amount of experimentally obtainable rate information on the three reactions. The standard deviation apparent in Figures 9 and 11 reflects the internal, or system, fluctuations characteristic of a mesoscopic system (such as van Kampen, 1992, p. 232–235). Since a system usually operates under the influence of external variables, the experimentally observed fluctuations should be greater than the internal fluctuations predicted by the model. This also implies that it is worth cautioning ourselves not to replicate the experiments excessively in an attempt to reduce the scattering far beyond what is predicted. By the same token, a few observed low concentrations can be a misleading indication of the termination of responses because the appreciable scattering, as discernable in Figures 9 and 11 portraying the standard deviation envelopes, signifies the influence of internal noises.

The current model adopts the essential concepts of the NSC model for analyzing the oxidation of a system containing a limited carbon source, thereby forming a closed system, that is, a carbon sheet; it has been chosen for analysis to illustrate the importance of the second stage. Nevertheless, it is worth noting that the master-equation algorithm is also applicable to the oxidation of open-flow systems, for example, the surface of a carbon rod. This algorithm involves the stochastic probability balance of the two types of clusters; the resultant master equation should yield not only the deterministic evolution of carbon clusters reported by Nagle and Strickland-Constable (1962), but also the fluctuations, or uncertainties, inherited in their measurement.

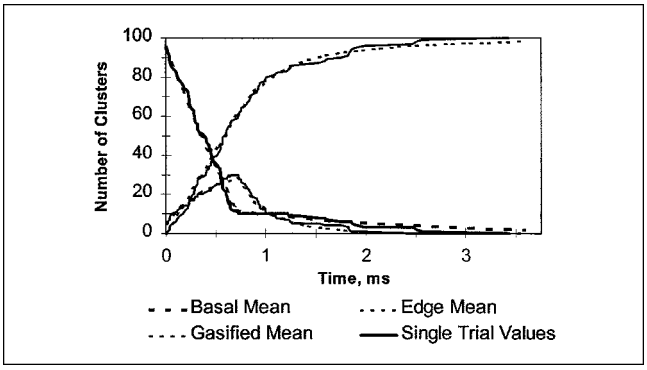

Figure 13. Mean trajectories generated by the master-equation algorithm and the single traces.

Simulated by the Monte Carlo algorithm for a carbon sheet containing 100 clusters.

Carbon oxidation leads to the removal of carbon from a solid matrix by oxygen into a gaseous phase, thereby resulting in pit formation on the surface of the solid; thus, the present analysis and model can also be applied to other processes involving pit formation, for example, corrosion, which has been treated as a stochastic birth and death process (such as Mola et al., 1990; Shibata, 1996). The present stochastic model, however, contains various features, such as the secondary, instantaneous conversion of basal sites to edge sites in the first stage and the separation of the entire process into two stages. Consequently, the model appears to be more suitable than the straightforward birth and death process for the analysis of pit formation.

Conclusions

The classic dual-site model of Nagle and Strickland-Constable for carbon oxidation has been successfully revised to take into account the stochastic nature of the process and the shift in the mechanism during the later stage. Carbon sheet, which is the simplest among the representative systems having limited carbon, is selected for the current study. The transition-intensity functions of the dynamic gasification and transformation of basal and edge clusters of carbon have been estimated through a stochastic analysis of the resultant two-stage model. Subsequently, this has given rise to the master equations for analytical representation and to the event-driven Monte Carlo procedure for numerical representation of the model. The master equations are capable of estimating not only the evolution of means of cluster numbers, but also the variances, or fluctuations, around the means in both stages. These fluctuations are inherent in the system and are attributable mainly to the mesoscopic defects of the carbon structure, which have been demonstrated experimentally as a potential source of uncertainties in determining the oxidation rates.

The validity of the model is amply demonstrated by numerically calculating the evolution of cluster numbers of different types and their fluctuations over time through two simulation algorithms, one based on the master equations and the other based on the event-driven Monte Carlo procedure. These two algorithms have been implemented separately but with the same set of assumptions and system parameters. The fact that the two algorithms have yielded essentially identical results implies that both define the evolution of a dynamic process in an equivalent way.

Notation

$E[N_i(t)]$ = expected value, mean, or the first moment of the random variable, $N_i(t)$
$E[N_i^2(t)]$ = second moment of the random variable, $N_i(t)$
$E[N_i(t)N_j(t)]$ = second, or product, moment of the random variables, $N_i(t)$ and $N_j(t)$
$f(u)$ = probability-density function of U
n_i = realization of the random variable, $N_i(t)$

Literature Cited

Blyholder, G., J. S. Binford, Jr., and H. Eyring, "A Kinetic Theory for the Oxidation of Carbonized Filaments," *J. Phys. Chem.*, **62**, 263 (1958).

Casella, G., and R. L. Berger, *Statistical Inference*, Pacific Grove, CA (1990).

Chiang, C. L., *An Introduction to Stochastic Processes and Their Applications*, Krieger, Huntington, NY, pp. 208, 447 (1980).

Chu, X., and L. D. Schmidt, "Reactions of NO, O_2, H_2O, and CO_2 with the Basal Plane of Graphite," *Surf. Sci.*, **268**, 325 (1992).

Chu, X., and L. D. Schmidt, "Intrinsic Rates of NO_x-Carbon Reactions," *Ind. Eng. Chem. Res.*, **32**, 1359 (1993).

Essenhigh, R. H., "Fundamentals of Coal Combustion," *Chemistry of Coal Utilization, Second Supplementary Volume*, Wiley, New York, p. 1278 (1981).

Felder, W., S. Madronich, and D. B. Olson, "Oxidation Kinetics of Carbon Blacks over 1300–1700 K," *Energy Fuels*, **2**, 743 (1988).

Gardiner, C. W., *Handbook of Stochastic Methods for Physics, Chemistry, and Natural Sciences*, 2nd ed., Springer-Verlag, Berlin (1985).

Gillespie, D. T., "Exact Stochastic Simulation of Coupled Chemical Reactions," *J. Phys. Chem.*, **81**, 2340 (1977).

Gillespie, D. T., *Markov Processes*, Academic Press, San Diego (1992).

Kyotani, T., K. Ito, A. Tomita, and L. R. Radovic, "Monte Carlo Simulation of Carbon Gasification Using Molecular Orbital Theory," *AIChE J.*, **42**, 2303 (1996).

Laine, N. R., F. J. Vastola, and P. L. Walker, Jr., "The Importance of Active Surface Area in the Carbon-Oxygen Reaction," *J. Phys. Chem.*, **67**, 2030 (1963).

Laurendeau, N. M., "Heterogeneous Kinetics of Coal Char Gasification and Combustion," *Prog. Energy Combust. Sci.*, **4**, 221 (1978).

Lizzio, A. A., H. Jiang, and L. R. Radovic, "On the Kinetics of Carbon (Char) Gasification: Reconciling Models with Experiments," *Carbon*, **28**, 7 (1990).

Mola, E. E., B. Mellein, E. M. Rodriguez de Schiapparelli, J. L. Vicente, R. C. Salvarezza, and A. J. Arvia, "Stochastic Approach for Pitting Corrosion Modeling: 1. The Case of Quasi-Hemispherical Pits," *J. Electrochem. Soc.*, **137**, 1384 (1990).

Nagle, J., and R. F. Strickland-Constable, "Oxidation of Carbon Between 1000–2000°C," *Proc. Conf. on Carbon*, Vol. 1, Pergamon Press, New York, p. 154 (1962).

Neoh, K. G., J. B. Howard, and A. F. Sarofim, "Soot Oxidation in Flames," *Particulate Carbon: Formation during Combustion*, D. C. Siegla and G. W. Smith, eds., Plenum, New York, p. 261 (1981).

Nicolis, G., and I. Prigogine, *Self-Organization in Nonequilibrium Systems*, Wiley-Interscience, New York, p. 223 (1977).

Oppenheim, I., K. E. Shuler, and G. H. Weiss, *Stochastic Process in Chemical Physics: The Master Equation*, The MIT Press, Cambridge, MA (1977).

Park, C., and J. P. Appleton, "Shock-Tube Measurements of Soot Oxidation Rates," *Combust. Flame*, **20**, 369 (1973).

Parzen, E., *Stochastic Processes*, Holden-Day, San Francisco (1962).

Petzold, L. R., and A. C. Hindmarsh, "A Systematized Collection of ODE Solvers," Lawrence Livermore National Laboratory Rep. (also available at http://www.netlib.org/odepack/doc) (1997).

Rajamani, K., W. T. Pate, and D. J. Kinneberg, ''Time-Driven and Event-Driven Monte Carlo Simulations of Liquid-Liquid Dispersion: A Comparison,'' *Ind. Eng. Chem. Fundam.*, **25**, 746 (1986).
Shibata, T., ''Statistical and Stochastic Approaches to Localized Corrosion,'' *Corrosion*, **52**, 813 (1996).
Spokes, G. N., and S. W. Benson, ''Oxidation of a Thin Film of a Carbonaceous Char at Pressures below 10^{-4} Torr,'' *Fundamentals of Gas-Surface Interactions*, H. Saltsburg, J. N. Smith, Jr., and M. Rogers, eds., Academic Press, New York, p. 318 (1967).
Suuberg, E. M., ''Thermally Induced Changes in Reactivity of Carbons,'' *Fundamental Issues in Control of Carbon Gasification Reactivity*, J. Lahaye and P. Ehrburger, eds., Kluwer, Dordrecht, The Netherlands, p. 269 (1991).
van Kampen, N. G., *Stochastic Process in Physics and Chemistry*, 2nd ed., Elsevier, Amsterdam (1992).
von Fredersdorff, C. G., and M. A. Elliott, ''Coal Gasification,'' *Chemistry of Coal Utilization*, Supplementary Volume, H. H. Lowry, ed., Wiley, New York, p. 892 (1963).

Manuscript received Nov. 6, 1998, and revision received July 26, 1999.

See NAPS document no. 05533 for 27 pages of supplementary material. This is not a multiarticle document. Order from NAPS c/o Microfiche Publications, 248 Hempstead Turnpike, West Hempstead, NY 11552. Remit in advance in U.S. funds only $18.50 for photocopies or $5.00 for microfiche. There is a $25.00 invoicing charge on all orders filled before payment. Outside the U.S. and Canada, add postage of $4.50 for the first 20 pages and $1.00 for each of 10 pages of material thereafter, or $5.00 for the first microfiche and $1.00 for each fiche thereafter.